Chapter 4
MXene-Derived Composites and Their Application in Energy Storage and Catalysis

Rayees Ahmad Rather and Rameez Ahmad Mir

4.1 Introduction

Recent advances in materials science have demonstrated the development of composites between different materials as an effective approach to stimulate their activity. Composites are preferably developed by blending two or more material entities with variable thermodynamic, oxidation, and reduction properties to promote their efficiency for some specific applications. The composite formation is a striking strategy for enhancing stability, mechanical, electrical, and thermal properties of any material. In light-driven reactions, this strategy effectively promotes the lifetime of excited charge carriers. In recent years, composites of two-dimensional (2D) materials especially graphene [1, 2] had revealed their potential for several critical applications credited to their layered, flexible, and tunable structural features. However, the issues pertaining to production cost, fragility, and environmental concerns encouraged researchers to explore analogous metal-based layered structures. In this regard, the research progress in transition metal dichalcogenides (TMDCs) and transition metal carbides/nitrides (TMCs/TMNs) exploded as a research boom in 2D materials research specifically in the field of energy conversion and storage [3]. Among the latest and most advanced materials, MXenes have emerged [4] as an unconventional 2D material with the possibility of wider applicability in composite formation due to their layered structure, distinctive surface properties, and tunable morphology. MXenes, a special class of 2D layered TMCs/TMNs discovered by Gogtsi et al. in 2011 [5] are flexible structures that are ideal for forming multifunctional materials. MXenes are primarily composed of carbides, nitrides, and carbonitrides obtained

R. A. Rather (✉)
Department of Civil, Construction, and Environmental Engineering, San Diego State University (SDSU), San Diego, CA 92182, USA
e-mail: rrather@sdsu.edu; rzr0074@auburn.edu

R. A. Mir
School of Engineering, University of British Columbia (UBC), Okanagan, Canada

O. P. Pandey and P. Sharma (eds.), *MXenes: Emerging 2D Materials*,
https://doi.org/10.1007/978-981-97-4064-2_4

by selective etching of the MAX phase, where M is transition metal, A represents group IIIA or IVA elements and C is carbon or nitrogen. MXenes have a general formula, $M_{n+1}X_nT_n$ ($n = 1$–3) where M and X are the same as in the MAX phase and T is the respective functional group (–O–, –OH, and –F). MXenes are versatile materials that exhibit a combination of metallic and ceramic properties, making them suitable for use in a variety of applications such as batteries, energy storage, catalysis, sensors, capacitors, etc. [6, 7]. The electrical, optoelectronic, and induction properties of MXenes are optimized based on the ratio of M, X atomic species, which amenably improves their energy conversion and storage performance [8, 9]. In addition, MXene-based supercapacitors and batteries exhibit high energy storage performance even when the electrolyte contains larger cations because the wider spacing between the MXene layers allows easy intercalation and deintercalation of these larger ions. As a result, the larger ions can effectively store and release energy within the MXene layers [10, 11].

However, several issues in MXenes such as restacking of layers, oxidation of specific species, and reduced electrical conductivity of certain functional groups in out-of-plane directions constrain their performance not only in energy storage systems but also in other catalytic applications. The poor Vander Waals interactions between MXene layers tends to effect their mechanical properties thus limiting their use in electronic applications. To overcome these limitations, researchers have developed composites of MXenes with other potential materials, such as polymers, metals, and carbon-based materials. The blend of these materials possess improved mechanical strength, electrical conductivity, electrochemical and catalytic performance over their individual counterparts. However, the choice of the composite materials determines its potential application, for example, MXene/polymer composites can be used as flexible electrodes for energy storage devices, while MXene/metal composites can be used as catalysts for several reactions.

In this regard, this chapter presents a descriptive outlook of the MXene-based composites, their synthesis, and role in different energy storage and catalysis applications.

4.2 Synthesis of MXene Composites

The synergism between MXene and hetero material in a composite is decided based on certain factors such as (1) type of interfacial contact, (2) characteristics of space charge region, (3) interfacial electron transfer, (4) accessible surface area, and (5) path length, from electron transition level to its interaction with the adsorbed chemical entity. Therefore, these factors are usually considered while fabricating a functional MXene composite. Numerous procedures and techniques have been adopted for the synthesis of novel MXene composites.

Figure 4.1a, shows several reported composites of MXenes including with polymers [12], metal oxides [13], mesoporous carbon (mC) [14], graphene (atomic layer graphene, graphene oxide (GO), reduced GO (rGO) [15], carbon nitride (C_xN_y) [16],

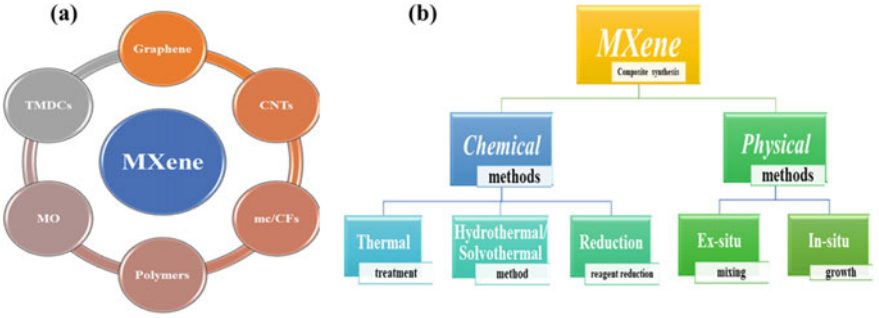

Fig. 4.1 **a** Schematic representation of different MXene composite species and **b** synthesis methods adopted

carbon nanotubes (CNTs) [17], and metal chalcogenides (TMDCs) [18]. Based on the type of additive material (0D, 1D, 2D, and 3D materials) and the intended end applications of the MXene composite, various synthesis protocols have been employed for composite formation (Fig. 4.1b).

Both chemical and physical methods are preferred for the synthesis MXene composites. However, the application requirement specifically determines the route of synthesis. Physical methods such as in-situ and ex-situ techniques are used for the development of a variety of MXene composites, as they avoid the formation of any impure phases or defects during the synthesis process.

In-situ composite synthesis involves the simultaneous formation of MXene and another material when precursors are subjected to reaction in a defined molar ratio. This method allows an integration of different functionalities of MXene and corresponding composite material enabling a significant change in the electrical and photoelectrical properties of the MXene composite. The in-situ process is a combination of several individual steps such as (1) precursor selection, (2) etching, (3) delamination, (4) addition of another composite component, (5) mixing and stabilization, (6) washing and drying. Typically etching and stabilization are two primarily important steps to regulate the formation of MXene structure and aggregation of particles. Characteristically, electrochemical and non-covalent interactions have been determined as the responsible forces for the formation of in-situ development of MXene composites [19].

In comparison to the in-situ method, the ex-situ route is a simpler procedure that involves the separate synthesis of MXene material and its subsequent mixing or dispersion into a matrix material in specific molar ratios to enable the interlayers of MXene to create a hybrid phase and enhance the overall activity of the composite. In ex-situ method, the etching is done on MAX phase only while as the dispersion and stability procedure remains like in-situ method. The ex-situ route involves the mixing or dispersion of MXene into different matrix materials such as polymers, metal oxides, carbonaceous materials, etc. In both cases, the developed hybrid composites exhibit higher interlayer spacing as compared to pure MXene [20, 21]. Additionally,

multilayer MXenes, single layer is more efficient due to better surface hydrophilicity and compatibility with other materials.

Apart from the metal oxide, the MXene composites with other materials such as graphene and carbon nanotubes were also reported for several charge transfer reactions. In a study by Xu et al. [22], an electrochemical approach was used to develop flexible all-solid-state supercapacitors (SCs) made of a graphene oxide (rGO)/$Ti_3C_2T_x$ film, utilizing rGO as a binder to link the active conducting particles. Thick electrodes with high electrolyte accessibility were developed without the need for any special procedures to delaminate the MXene layers. The resulting composite material exhibited a higher specific capacitance than the individual ingredients (GO, rGO, or MXene).

In contrast to physical methods, chemical methods crucially improve the physicochemical and thermomechanical properties of MXene composites. The strength of the composite is determined by the hydrogen bonding between the negative charge of the functional group (–T) on the surface of MXene and the compounding species. The bonding and tailoring of the –T group with the composite species determine the utilization of the MXene composite for respective applications. Among the various additive materials used for MXene composite formation, carbon materials such as mesoporous carbon (mC), carbon fibers (CFs), carbon nanotubes (CNTs), and graphene have received special attention due to their easy availability, high surface area, and distinctive surface characteristics that work in larger voltage windows and possess better adsorption and charge transfer ability.

4.3 Applications of MXene-Derived Composites

MXene-based composites are being extensively explored to catalyze wide range of electronic and energy applications due to their unique electrokinetic, optoelectronic and storage properties. MXene derived composites offer higher effective surface area, high density of active sites, effective charge and mass transport. Majorly, the MXene-based composites are being tested for the following applications.

1. *Energy storage*: The MXene composites have high effective surface redox sites and conductivity, which makes them ideal for use in energy storage devices such as batteries and supercapacitors.
2. *Catalysis*: MXene based composites can be used as catalysts to drive several electrochemcial, thermal and photocatalytic reactions due to their high surface area and unique surface chemistry. MXene composites not only acts as the co-catalysts for certain reactions, but they also act as support for adsorption and promote the charge and mass transfer process. Therefore, MXene composites have the potential to promote the efficiency and yield in several environmental remediation and renewable energy processes.

3. *Water purification*: MXene composites are suitable adsorptive photocatalytic materials for sustainable treatment of heavy metals, organic pollutants and other recalcitrant pollutants.
4. *Biomedical applications*: MXene composites have potential applications in biomedical fields such as sensors, drug delivery, tissue engineering, and biosensing due to their biocompatibility and unique properties.

The MXene composites have a tremendous potential to scale up the efficiency of different reactions across different domains. However, in this chapter, a descriptive outlook of these composites for energy storage and catalysis is presented.

4.3.1 MXene Composites for Energy Storage

MXene composites are appropriate materials for energy storage and conversion applications due to their exceptional structural, morphological, and electrical properties. Research efforts are focused on optimizing the synthesis techniques to specify the molar ratios and enhance the chemical and electrostatic compatibility of individual ingredients in MXene composites, which in turn will improve the scalability of production which is a prerogative for practical implementation of these composites in energy storage and conversion applications.

Among various competitive options, the graphene-based MXene composites have gained significant attention due to their layered structures and high conductivity. These composites are attractive because they not only enhance performance by leveraging the superior properties of graphene but also maintain the unique two-dimensional structure of the composite, which further improves its overall activity and stability. The synergism and combination between MXene and graphene is a noteworthy, particularly with regards to the alignment of neighboring crystals, interface quality, and the abundance of edge sites. Zhou et al. [23] investigated the $Ti_3C_2T_x$ MXene phase to functionalize reduced graphene oxide (rGO) sheets through Ti–O–C covalent bonding, which was crosslinked by 1-aminopyrene-disuccinimidyl (AD) substrate to enhance the compactness and toughness of the resulting MXene-rGO (MrGO) sheets (Fig. 4.2a). A flexible symmetric supercapacitor was fabricated utilizing MrGO-AD sheets as electrodes (5 μm thick, 2 cm long, and 1 cm wide) and PVA/H_3PO_4 as the gel electrolyte (Fig. 4.2b). The developed cell demonstrated high cyclic stability even at a scan rate of 1000 mV s^{-1} (Fig. 4.2c). The supercapacitor performance estimated through GCD curves (Fig. 4.2d) exhibited volumetric capacitance of 645 F cm^{-3} at an applied current density of 1.0 A cm^{-3}. The cell also revealed a high stability with a capacitance retention of 75.3% at 8.6 A cm^{-3} and a high coulombic efficiency (CE ~100%) as shown in Fig. 4.2e, respectively. The capacitor also exhibited a very high cyclic stability with negligible loss of capacitance even after 20,000 CV cycles (Fig. 4.2f). The Ragone plot (Fig. 4.2g) revealed that the developed electrodes perform better than the commercial activated carbon (AC) and lithium (Li)

batteries. The supercapacitor based on MXene and rGO sheets provides a combination of high toughness and strength electrodes with energy/power density essential for developing the highly efficient and durable flexible supercapacitors. The results revealed that the improved performance of the capacitor can be attributed to the use of MXene and π-π bridging, which increases the alignment of the MXene-rGO sheets. The capacitor's performance was evaluated at different bending angles (0°, 90°, and 180°), and it was found that bending and twisting did not affect its performance. Additionally, combining the three electrodes in series improved the voltage range threefold compared to using individual electrodes, providing a path to develop multilayer cells for practical applications. However, to further enhance the performance of the supercapacitors, it is crucial to consider ion accessibility on the electrode sites. The ion exchange transfer kinetics are notably low in organic electrolytes, especially at low temperatures (below freezing). Addressing this issue can lead to significant improvements in the performance of MXene-rGO-type supercapacitors.

The accessibility of the electrolyte ions in the electrodes plays a vital role for enhancing the charge storage performance especially at low temperatures. In this

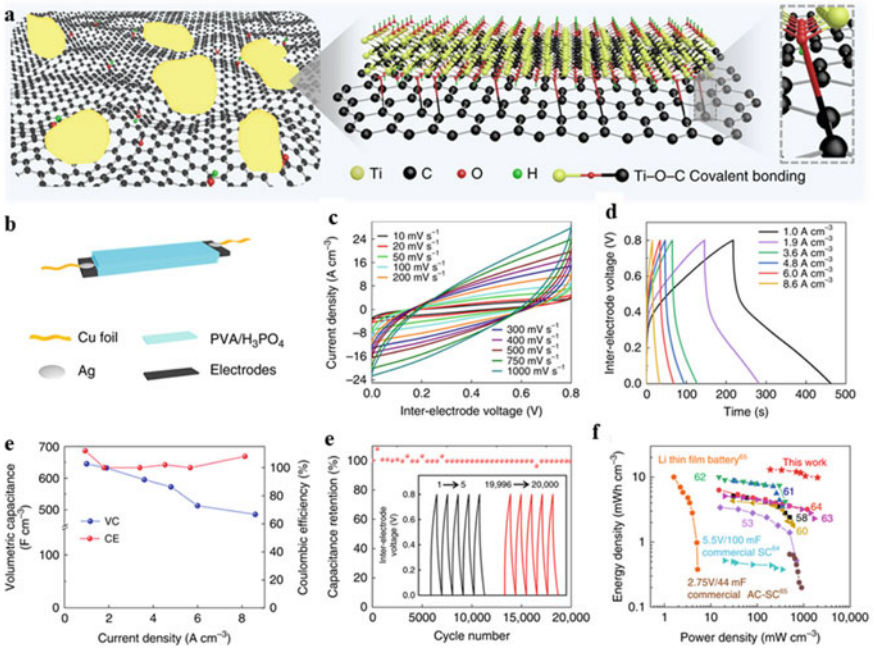

Fig. 4.2 **a** Schematic model of MXene-GO platelets showing the formation of Ti–O–C covalent bonding, **b** illustration of the components of a flexible supercapacitor based on MrGO-AD sheets. **c** Cyclic voltammetry (CV) curves at scan rates of 10–1000 mV s^{-1} for the MrGO-AD supercapacitor. **d** GCD curves for the MrGO-AD sheet supercapacitor. **e** Volumetric capacitance of the MrGO-AD sheet supercapacitor for current densities from 1.0 to 8.6 A cm^{-3}. **f** Capacitance retention during the cycling of a MrGO-AD supercapacitor. Figure adopted with permission from [23]

regard, Gao et al. [24] developed MXene knotted CNT composite as a high-rate performance electrodes (Fig. 4.3a–c). The breakage of the 2D alignment of the Ti_3C_2 MXene sheets by the special CNT knots prevents the restacking of the sheets and creates fast ion transport pathways. The capacitor performance of the MXene composite was tested through three and two electrodes set up in an organic electrolyte. The synthesized Ti_3C_2/CNT composite exhibited a capacitance performance of 128 F g^{-1} at 1 A g^{-1}. To check the performance of the composite at low operating temperatures, the asymmetric cell was fabricated with Ti_3C_2/CNT with 17% CNT composite as negative electrode and aligned CNT as positive electrode (Fig. 4.3d), respectively. The CV at multiple scan rates in a wide voltage window (0–3 V) shows a negligible loss of capacitance even at higher scan rates as shown in Fig. 4.3e. The quasi-rectangular shape of CV curve and symmetric shape of GCD curves (Fig. 4.3f) without a plateau reveals the pseudocapacitive behavior of the composite material. The asymmetric capacitor exhibited a capacitance of 130 F g^{-1} higher than aligned CNTs (94 F g^{-1}) and showed capacitance retention of more than 90% even after 8000 cycles. The cell capacitance at lower operating temperature (Fig. 4.3g) shows that capacitance decreased by 50% as compared that performed at 20 °C. The absence of the redox peaks at lower temperatures (Fig. 4.3h) shows that the double-layer mechanism is responsible for charge storage. The operational voltage window up to 4.2 V is higher than that achieved in activated carbon materials (3 V). The highest capacitance retention was observed in composite material with 9% CNT as compared to 17% (Fig. 4.3i) and bare MXene, respectively. The results suggested that conductivity plays a vital role on capacitive performance of the cell at lower operating temperatures. An impressive capacitance, energy density (59 Wh kg^{-1}), and a power density (9.6 kW kg^{-1}) were obtained at −30 °C. The performance is better than the values reported for supercapacitors with 2D electrode materials operating at low temperatures. The study has demonstrated that MXene/carbon composites made from pseudocapacitive materials can be utilized for high-rate energy storage in organic electrolytes by optimizing the electrode architecture. This is due to the exceptional hydrophobicity and conductivity of the MXene/graphene composites, which has led to extensive efforts to enhance their supercapacitor performance. Despite their potential, the use of MXene/graphene composites in practical applications is still limited by several factors, such as the complicated synthesis process and the high cost associated with the use of graphene [15].

To deliver on such bottlenecks, conductive polymers have garnered significant interest as alternative additive composite materials for creating flexible, lightweight, and conductive MXene/polymer composites that serve as electrodes for energy storage devices [25–27]. Adekoya et al. [28] conducted a study on the effects of polypyrrole (PPy) polymer on the properties and performance of MXene/PPy nanocomposites. However, to fabricate the MXene/PPy composites, in-situ polymerization is considered as a promising approach. Various types of flexible MXene/PPy composite electrodes were designed and fabricated. Furthermore, an in-depth investigation and comparison studies of MXene/PPy composites revealed that the incorporation of PPy enhances both the stability and the energy storage performance. Similarly, Li et al. [29] fabricated a textile-based electrode made of polyester fabric

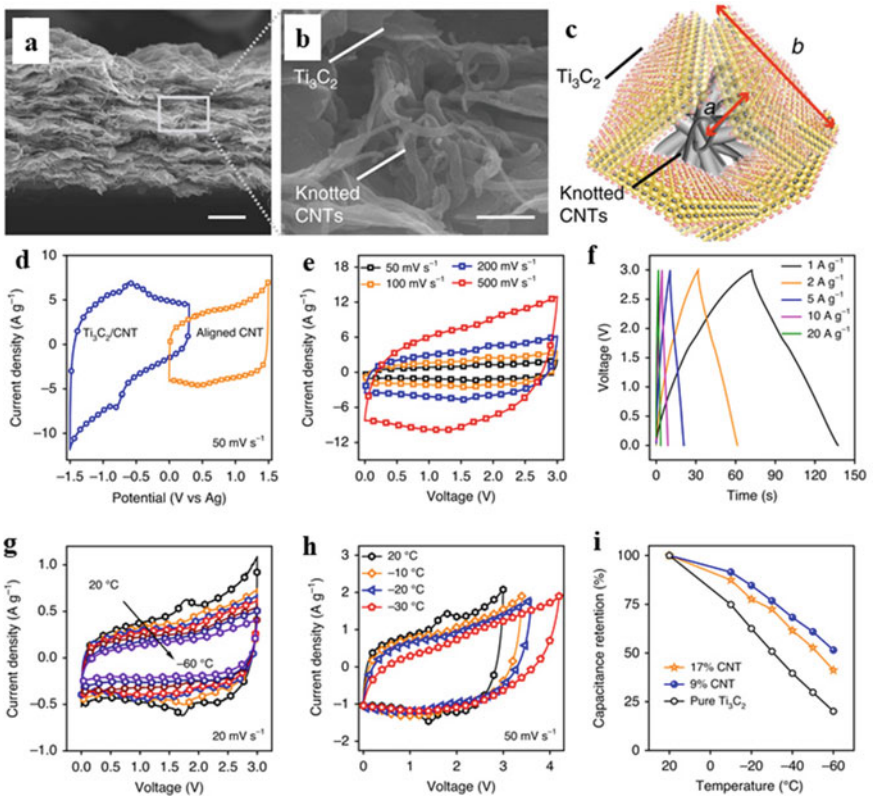

Fig. 4.3 **a** Cross-sectional SEM images of an MXene-knotted CNT composite electrode with 17% CNTs, **b** SEM image of composite, **c** schematic illustration of the Ti_3C_2 flakes was broken by the knotted CNTs to form 3D networked structure. "a" and "b" (~1:2 ratio), **d** full cell fabrication: three-electrode CVs of the MXene-knotted CNT (Ti_3C_2/CNT) composite electrode and aligned CNT electrode at 50 mV s^{-1}, **e** cyclic voltammograms for the full cell at different scan rates, **f** galvanostatic charge–discharge curves for the full cell at different current densities, **g** cyclic voltammograms at different temperatures at 20 mV s^{-1}, **h** cyclic voltammograms with larger voltage windows at low temperatures for the full cell using MXene-knotted CNT composite electrode with a CNT content of 17% as the negative electrode, and **i** capacitance retention of full cells with different Ti_3C_2 MXene-based electrodes as a function of temperature. Figure adopted with permission from Ref. [24]

modified with polyethyleneimine (PEI) Mxene/PPy composite (PPy/MXene/PMFF). The capacitor performance of the developed composite was estimated by a symmetric cell procedure with PPy/Ti_3C_2/PMFF as electrodes and advanced PVA/Na_2SO_4 gel as electrolyte. The polymer-encapsulated MXene provides more abundant sites and modified channels for electron transport to improve the capacitive performance. Based on the mass loading of the active material (PPy/MXene), the PPy/MXene/PMFF composite revealed a real capacitance of 1295 mF cm^{-2} and a gravimetric capacitance of 439 and 360 F g^{-1} at 1 and 50 mA cm^{-2}, respectively. Moreover, the

polymer/MXene composite exhibited excellent stability with no significant drop in capacitance even at higher scan rates. The designed electrode shows only a drop of 6.3% in overall capacitance after 30,000 cycles. The higher rate performance, high energy/power density, high stability even different deformation angles, and excellent cyclic stability contribute to the significant advances in textile-based electrodes for wearable electronic devices. The comparison studies of different MXene polymer composites and their respective performance are given in Table 4.1.

Moreover, to improve the number of redox sites and enhance the performance of MXene electrodes, the synthesis of MXene/TMO composites is considered a promising approach. Typically, TMOs made of metals such as Manganese (Mn), Vanadium (V), Iron (Fe), Nickel (Ni), and Cobalt (Co) have been explored due to their high theoretical capacity, wide availability, low cost, multiple oxidation states, and higher number of redox sites. Various transition metal oxide-based MXene composites (MXene/TMOs) have been developed as electrode materials for supercapacitors, as presented in Table 4.1 [30].

However, despite the higher capacitance and energy density observed in the developed supercapacitors (SCs), still fall short of the energy density values obtained in batteries. To further improve the pseudocapacitive performance of the MXene electrodes, Wang et al. [31] produced a tungstate/MXene composite electrode for use in lithium and sodium-ion batteries. The electrode was free-standing and aligned to minimize ion-path tortuosity, enhancing ion transport, and ultimately leading to improved efficient pseudocapacitive storage performance. The developed flexible electrodes demonstrated high capacity and long-term performance, with a capacity of 267.0 mAh g^{-1} observed in the case of Li-ion batteries and a CE greater than 78%. Even at various deformation angles, negligible loss of capacity was observed. These results suggest the potential application of the developed composite material in wearable electronic devices.

In addition, energy storage properties of transition metal oxide/MXene composites were enhanced by increasing the number of redox-active sites due to the incorporation of metal oxide species, especially those of Ni, Co, Sn, and Fe-oxides. The charge storage mechanism in batteries is diffusion-controlled and depends on the redox reactions occurring deep within the electrode material. However, the charge storage mechanism is surface controlled process. A study presented by Wang et al. [32] showed a composite electrode consisting of carbon-coated iron oxide (Fe_3O_4) nanoparticles (C@Fe_3O_4 NPs) decorated on Ti_3C_2/MXene for Li-ion battery applications. Fe_3O_4 was chosen as an additive due to its high theoretical capacitance of 3625 F g^{-1}. The uniform distribution of C@Fe_3O_4 NPs improved the specific surface area from 7.8 to 30 m^2 g^{-1}. The C@Fe_3O_4 NPs/Ti_3C_2 composite exhibited a higher capacity of 231.5 mAh g^{-1} as an anode in Li-ion batteries compared to pristine Ti_3C_2 MXene (107.8 mAh g^{-1}). Similarly, Liu et al. [33] used the hydrothermal reaction route to develop VO_2-enriched V_2CT_x MXene as an electrode for Li-ion batteries. The partially etched V_2CT_x MXene phase was oxidized in the presence of H_2O_2 to enhance the layer spacing of the resultant oxidized phase as shown in Fig. 4.4a. The presence of the VO_2 phase was confirmed by the XRD pattern (Fig. 4.4b) and the enhancement of the layer spacing before and after hydrothermal treatment was

Table 4.1 Electrochemical performance of MXene/composite-based SCs. Adopted with permission from Refs. [15, 30]

Electrode(s)	Electrolyte	Capacitance	Current density	Retention (%)	Number of cycles
MXene/rGO composite	2M KOH	154.3 F g^{-1}		85	6000
MXene/rGO films	6M KOH	405 F g^{-1}		No change	10,000
MXene/rGO hybrid fiber	1M H_2SO_4	370 F cm^{-3}		No change	3000
MXene/rGO films	3M H_2SO_4	586.4 F cm^{-3}		No change	20,000
MXene/rGO composite aerogel	1M H_2SO_4	1040 F cm^{-3}		91	15,000
MXene/holey rGO composite	3M H_2SO_4	438 F g^{-1}		93	10,000
Co-MXene/rGO hybrid aerogel	6M KOH	345 F g^{-1}		85	10,000
MXene/rGO hydrogels	Saturated K_2SO_4	370 F g^{-1}		–	–
Mxene/MnO_2	Na_2SO_4	312 F cm^{-3}	5 mV s^{-1}	130.8	5000
MnO_2/Mxene	KOH	611.5 F g^{-1}	1 A g^{-1}	96	1000
Mxene/MnO_2 NR	KOH	130.5 F g^{-1}	0.2 A g^{-1}	100	1000
Mxene/MnO_2 NS	Na_2SO_4	340 F g^{-1}	1 A g^{-1}	87.6	2000
Mxene/Fe_3O_4	Li_2SO_4	46.4 mF cm^{-2}	0.5 mA cm^{-2}	96.3	85,000
MnO_2/Mxene NW	KOH	212 F g^{-1}	0.1 A g^{-1}	88	10,000
Co-Fe oxide/$Ti_3C_2T_x$	LiCl	2467.6 F cm^{-3}	0.2 mA cm^{-2}	88.2	10,000
$Ti_3C_2T_x$/Fe_2O_3	LiCl	405.4 F g^{-1}	2 A g^{-1}	97	2000
TiO_2/Mxene	KOH	143 F g^{-1}	5 mV s^{-1}	96	3000
V_2O_5/MXene	$LiNO_3$	217 F g^{-1}	0.1 mA cm^{-2}	104	5000

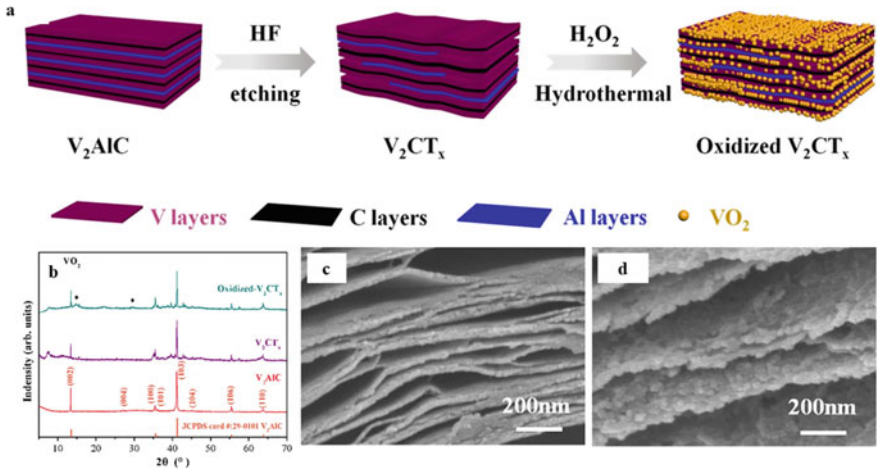

Fig. 4.4 **a** Schematic illustration of the synthesis of oxidized V_2CT_x, **b** XRD pattern, and **c–d** SEM images of the developed product. Adopted with permission from Ref. [33]

observed in the micrographs shown in Fig. 4.4c–d, respectively. The electrochemical tests were performed by fabricating a coin cell with oxidized V_2CT_x (80% by weight) as anode and Li-foil as cathode material. 1M $LiPF_6$ dissolved in (ethylene carbonate (EC), dimethyl-carbonate (DMC), and ethyl methyl carbonate (EMC) at a volume ratio of (1:1:1) as electrolyte and Celgard 2400 micro-porous membrane as separator.

The CV at a very low scan rate of 0.1 mV s^{-1} as shown in Fig. 4.5a (V_2CT_x), and Fig. 4.5b (oxidized V_2CT_x) shows the presence of redox peaks in the pristine MXene phase. However, the peaks disappeared in the oxidized phase which attributes to fact that the presence of O-terminated groups and VO_2 phase improved the Li^+ capture and improved the reversibility of the reactions during CV cycling. The specific capacity estimated at varying current densities in the oxidized V_2CT_x phase is higher than the pristine MXene and MAX phase (Fig. 4.5a–c). The rate performance (Fig. 4.5d) of the oxidized MXene reaches up to 318 mAh g^{-1}, which is more. The results revealed that the increased layer spacing in the oxidized phase plays a key role in the Li-intercalation/deintercalation process to increase the charge storage performance. However, for practical applications, cycling stability and long-term performance retention are necessarily required. The capacity of the MXene phase decreased for the first 100 cycles as shown in Fig. 4.5e. This decrease corresponds to the improved Li^+ accessibility with the number of cycles. The presence of the oxide terminated groups improves the reversible capacities than the pristine MXene. The VO_2 phase formed in the oxidized MXene (V_2CT_x) acts as the bridge between the V_2CT_x and Li^+, which provides more diffusion channels to improve the reversibility of the oxidized V_2CT_x phase. The oxidized V_2CT_x phase revealed an excellent stability up to 1000 cycles with negligible loss of capacitance as shown in Fig. 4.5f. The CE curve remained linear with no loss even after 1000 cycles.

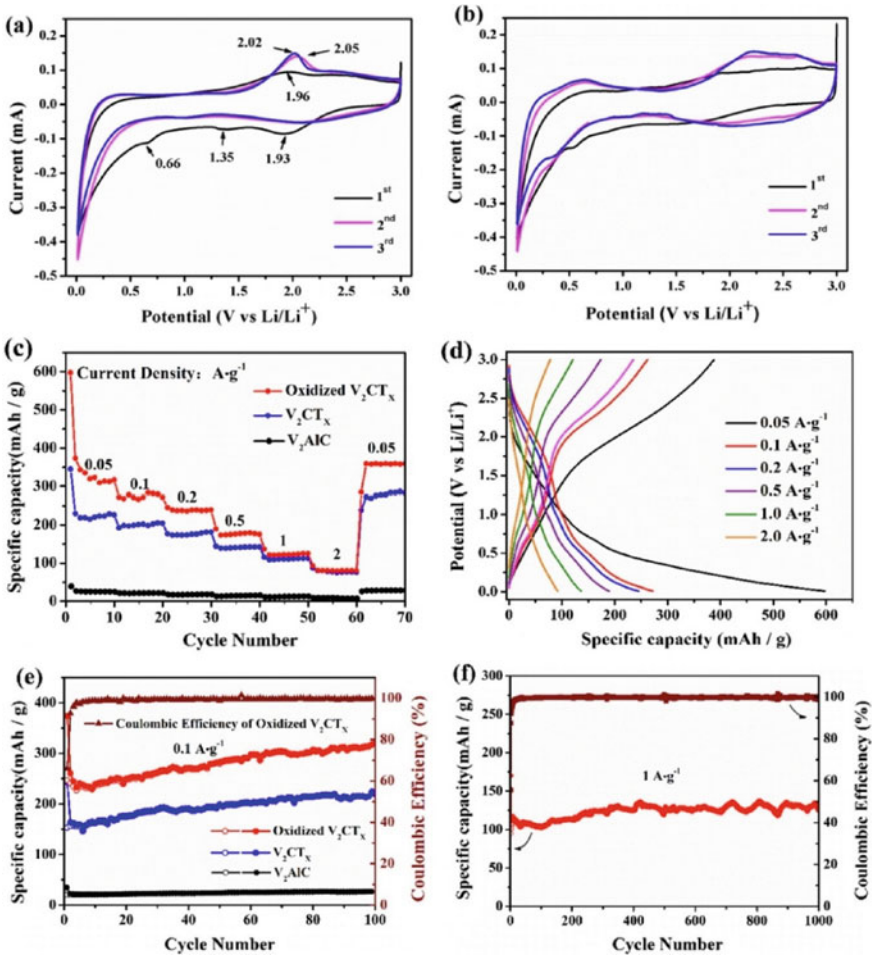

Fig. 4.5 The CV curves of V_2CT_x (**a**) and oxidized V_2CT_x **b** at 0.1 mV s^{-1} for the initial three cycles; **c** and **d** the rate performance at different current densities; **e** the cycle performance of V_2CT_x and oxidized V_2CT_x at a current density of 0.1 A g^{-1}. Adopted with permission from Ref. [33]

The oxidized V_2CT_x phase represented good performance stability and reversibility, justifying potential use as anode materials for lithium storage. Different other oxide materials have been tested along with MXenes as electrodes for Li, Na, and Zn batteries. The presence of the oxide materials as the composite additives improves both the activity and stability. The battery performance of the different MXene/TMO composite (Table 4.2) is higher than observed in pure V_2CT_x phase.

Table 4.2 MXene/TMO composite for battery applications. Adopted from Ref. [30]

Serial Number	MXene/TMOS material	First cycle capacity (mAh g^{-1})/ current density	First cycle capacity (mAh g^{-1})/current density	Last cycle capacity (mAh g^{-1})/ current density	Last cycle capacity (mAh g^{-1})/ current density
	$CoO/Co_2Mo_3O_8$@$Ti_3C_2T_x$	1008.8/0.1 A g^{-1}	936.2@100/0.1 A g^{-1}	545/2 A g^{-1}	1200
2	γ-Fe_2O_3@$Ti_3C_2T_x$	805.4/0.1 A g^{-1}	1060@400/0.5 A g^{-1}	466/2 A g^{-1}	800
3	Oxidized-V_2CT_x	318/0.05 A g^{-1}	318@100/0.1 A g^{-1}	125/1 A g^{-1}	1000
4	Fe_3O_4@$Ti_3C_2T_x$	517/0.2 C	–	236.7/5 C	300
5	SnO_2@$Ti_3C_2T_x$	829.4/0.2 A g^{-1}	829.4@100/0.2 A g^{-1}	533.9/1 A g^{-1}	500
6	Fe_3O_4@$Ti_3C_2T_x$	809.1/0.1 A g^{-1}	782.7@100/0.1 A g^{-1}	667.9/1 A g^{-1}	600
7	$Ti_3C_2T_x/TiO_2$	300/0.1 A g^{-1}	130@10/0.5 A g^{-1}	143/0.5 A g^{-1}	200
8	Fe_3O_4@$Ti_3C_2T_x$	954.7/0.5 A g^{-1}	701.8@200/0.2 A g^{-1}	609.9/0.5 A g^{-1}	600
9	$Co_3O_4/Ti_3C_2T_x$	1326/C/5	1005@300/1C	307	1000
10	TiO_{2-x}/Ti_3C_2	206/0.1 A g^{-1}	–	131/5 A g^{-1}	500
11	MXene-bonded Si@C	1660.6/ 0.42 A g^{-1}	–	1040/0.42 A g^{-1}	150
12	MXene derived TiO_2/Fe_2O_3	469.8/0.1 A g^{-1}	329.5@590/0.1 A g^{-1}	100/0.1 A g^{-1}	2000
13	Co_3O_4@s-$Ti_3C_2T_x$	747/0.1 A g^{-1}	550/@700/1 A g^{-1}	160/5 A g^{-1}	100
14	Cu_2O/Ti_2CT_x	790/0.01 A g^{-1}	–	143/1 A g^{-1}	250
15	SnO_2/Ti_2CT_x	736/0.5 A g^{-1}	–	258/0.5 A g^{-1}	50
16	$Li_4Ti_5O_{12}/Ti_2CT_x$	136/10 C	–	118/10 C	1000
17	N-doped TiO_2-MXene	305/0.03 A g^{-1}	–	369/0.03 A g^{-1}	100
18	$Ni_{0.8}Mn_{0.2}$-PBA/MXene	442/0.1 A g^{-1}	443@50/0.1 A g^{-1}	259.9	650
Zinc ion batteries (ZIBs)					
1	$Mn_xV_{10}O_{24}{\cdot}nH_2O$@$V_2CT_x$	424.4/0.5 A g^{-1}	358.2@300/1 A g^{-1}	289.6/10 A g^{-1}	25,000
2	CC@MnO_2@$Ti_3C_2T_x$	517/0.1 A g^{-1}	505.2@45/0.1 A g^{-1}	80.6/1 A g^{-1}	800

(continued)

Table 4.2 (continued)

Serial Number	MXene/TMOS material	First cycle capacity (mAh g^{-1})/ current density	First cycle capacity (mAh g^{-1})/current density	Last cycle capacity (mAh g^{-1})/ current density	Last cycle capacity (mAh g^{-1})/ current density
3	ZMO@$Ti_3C_2T_x$	~175/0.1 A g^{-1}	~175@100/0.1 A g^{-1}	172.6/1 A g^{-1}	5000
4	$H_2V_3O_8$/$Ti_3C_2T_x$	317.4/0.2 A g^{-1}	290.1@150/0.2 A g^{-1}	86.1/10 A g^{-1}	6600
5	3D $Ti_3C_2T_x$@MnO_2	301.2/0.1 A g^{-1}	–	202.2/0.1 A g^{-1}	2000
6	V_2O_5@V_2CT_x	397/0.5 A g^{-1}	~335@100/0.5 A g^{-1}	345/4 A g^{-1}	2000
7	V_2O_x@V_2CT_x	300/0.05 A g^{-1}	–	246/1 A g^{-1}	200
8	VO_x@V_2CT_x	423.5/1 A g^{-1}	398.1@80/5 A g^{-1}	283.7/30 A g^{-1}	2000
9	V_2CT_x@MnO_2	408.1/0.3 A g^{-1}	–	119.2/10 A g^{-1}	10,000
10	$(NH_4)_2V_{10}O_{25}\cdot 8H_2O$@ $Ti_3C_2T_x$	514.7/0.1 A g^{-1}	331.8@500/0.5 A g^{-1}	105.6/5 A g^{-1}	6000
11	VO_2/$Ti_3C_2T_x$	445/0.1 A g^{-1}	244.5@2600/ 20 A g^{-1}	225/30 A g^{-1}	4000
12	VO_2/$Ti_3C_2T_x$	228.5/0.2 A g^{-1}	–	126.6@2 A g^{-1}	700

4.3.2 MXene Composites for Catalysis

MXene composites had been reported as catalysts due to their unique physical and chemical properties. These composites have a high surface area, which provides many active and adsorption sites for catalytic reactions. Additionally, they exhibit excellent electronic conductivity and can act as conductive supports for catalyst nanoparticles. Several studies have reported the use of MXene composites as catalysts for various reactions. For example, $Ti_3C_2T_x$ composites have shown good performance for the oxygen evolution reaction (OER) and hydrogen evolution reaction (HER) [34]. These composites have shown excellent catalytic activity and stability, making them promising candidates for water electrolysis and other types of catalytically uphill reactions. Additionally, MXene composites were also used as catalysts for organic reactions like the reduction of nitroarenes or organic transformations [35]. The composites exhibited high catalytic activity and selectivity towards the desired reduction product, making them potential candidates for the synthesis of pharmaceuticals and agrochemicals. Three major domains where Mxene composites are

explored as potential catalysts include, (1) photocatalysis, (2) catalytic sensors, and (3) pollutant remediation.

4.3.2.1 MXene Composites as Photocatalysts

Photocatalysis is a process in which light is used to drive a chemical reaction [36], among the widely studied reactions, the infamous water splitting, hydrogen production, CO_2 reduction, and nitrogen fixation are the best specimen reactions with uphill thermodynamic requirements that researchers try to undo via photocatalytic approach [37, 38]. To achieve higher quantum conversion efficiency, the photocatalysts need to possess some exceptional characteristics such as (1) higher photoactivation response, (2) perennial stability and greater charge transfer ability, (3) lower recombination rate of excited electron–hole pairs, (4) efficient separation of charge carriers and their interaction with reactants adsorbed on the surface, and above all (5) suitable band profile to execute specific oxidation and reduction reactions. Single-component MXenes can't meet all the criteria to be an effective photocatalyst. However, the surface hydrophilic properties of MXene due to the presence of –OH and –O groups enable them to form suitable photocatalytic composite systems with other photoactive co-catalysts to drive some reactions. MXene composites have been used to drive numerous uphill reactions such as water splitting, CO_2 reduction and N_2 reduction.

An et al. [39] used a combination of Pt and Ti_3C_2Tx co-catalyzed C_3N_4 MXene composite for photocatalytic hydrogen production. The composite showed improved conductivity and exhibited an excellent photocatalytic response for hydrogen production (5.5 mmol h^{-1} g^{-1}). The higher performance is attributed to the MXene-facilitated effective charge transfer and separation of e^-/h^+ pair. Similarly, a combination of Ti_3C_2 and cadmium sulfide (CdS) MXene composite was reported for the photocatalytic hydrogen production [40]. The Ti_3C_2–CdS composite was prepared by hydrothermal synthesis route, the morphology and structural interpretation of the composite revealed a heterojunction between Ti_3C_2 and CdS (Fig. 4.6a–b). The composite produced 14.3 mmol h^{-1} g^{-1} of hydrogen equaling and apparent quantum efficiency of 40.1% (Fig. 4.6c). The performance of the composite is credited to suitably aligned band profile of the Ti_3C_2–CdS photocatalytic system leading to an interfacial electron transfer from CdS to Mxene along the formation of space charge region (Fig. 4.6d). A Schottky junction is formed (Fig. 4.6d) after the fermi level equilibration allowing electrons to shuttle towards Ti_3C_2 surface leaving behind the positive holes, the excellent conductivity or the MXene allows the water reduction to generate H_2 gas. Furthermore, as shown in Table 4.4, several MXene-based composites have been reported for photocatalytic hydrogen production under half reaction conditions. The performance in most cases is ascribed to the co-catalytic role of MXene in the composite leading to the effective separation and prolonged lifetime of excited electron hole pairs.

Moreover, MXenes composites have been reported for the photocatalytic CO_2 reduction to produce C1 fine chemicals as the products in a sustainable way. For example, Ti_3C_2 was utilized as a co-catalyst to enhance the photocatalytic response

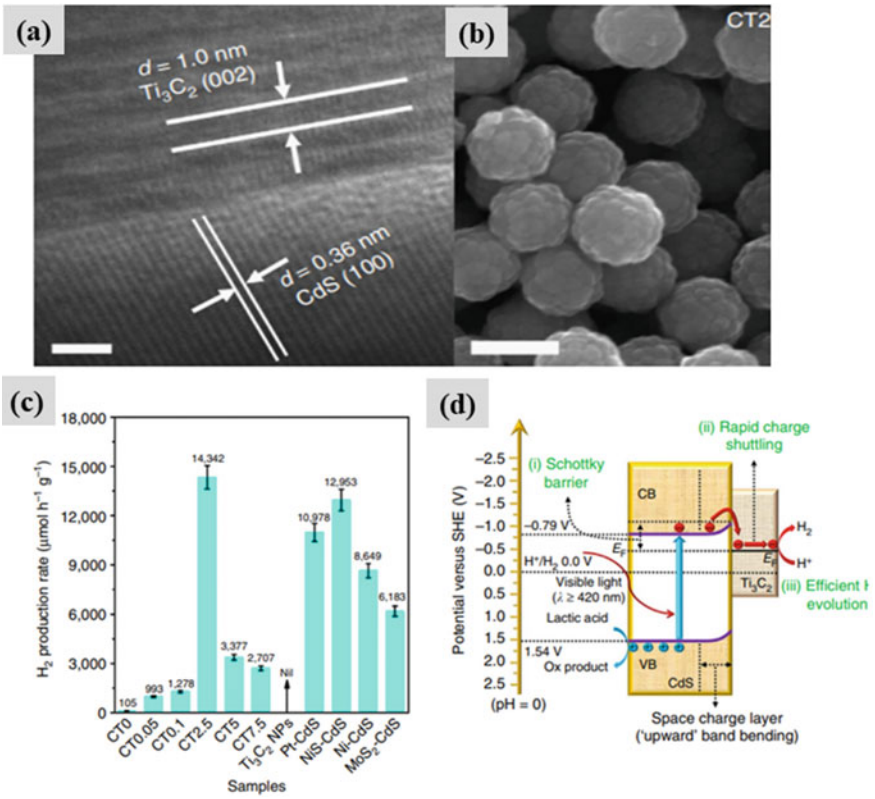

Fig. 4.6 **a** A high-resolution TEM image and **b** SEM image of CdS/Ti_3C_2 composite (CT2.5). **c** Photocatalytic activity of the CdS/Ti_3C_2 composite, **d** plausible mechanism of charge transfer in CdS/Ti_3C_2 under visible light irradiation. Adopted with permission from Ref. [40]

Table 4.4 Photocatalytic hydrogen production by different MXene composites in different reaction conditions and under visible light irradiation

MXene composite	Reaction medium	H_2 production ($\mu mol\ g^{-1}\ h^{-1}$)	Ref.
TiO_2 nanofibers/$Ti_3C_2T_x$	Water/Methanol	6979	[42]
$Ti_3C_2T_x$ nanoparticles/CdS	Water/Lactic acid	14,342	[40]
TiO_2 /$Ti_3C_2T_x$/CoS	Water/Methanol	950	[43]
C_3N4 /$Ti_3C_2T_x$/Pt	Water/TEOA	5100	[39]
g–C_3N_4@$Ti_3C_2T_x$	Water/TEOA	5111	[44]
ZnO nanorods /$Ti_3C_2T_x$	Water/Ethanol	456	[45]
CdS/MoS_2/$Ti_3C_2T_x$	Water/Sodium sulfate	9679	[46]
$CdLa_2S_4$/$Ti_3C_2T_x$	Water/Sodium sulfate	11,182	[47]
Ti_3C_2Tx/TiO_2/g–C_3N_4	Water/TEOA	1620	[48]
Mo_xS@TiO_2@$Ti_3C_2T_x$	Water/TEO/Acetone	10,505	[49]
Cu/TiO_2@Ti_3C_2T	Water/Methanol	764	[50]

of TiO_2 during a photocatalytic CO_2 reduction reaction [41]. As a result, the Ti_3C_2–TiO_2 composite produced CO (11.74 μmol g^{-1} h^{-1}) and CH_4 (16.61 μmol g^{-1} h^{-1}) as the reduction products. Again, the credit for the efficiency was attributed to the effective charge separation leveraged by the presence of MXenes. Several similar composites have been reported recently for the photocatalytic capture and conversion of CO_2 to fine chemicals.

4.3.2.2 MXene Composite Sensors

Studies have revealed that 2D materials are most popular for sensor and wearable applications due to their novel physical, morphological, and optoelectronic properties [51]. MXenes being a 2D class of layered materials have the potential tendency in sensor applications as they possess huge surface area, excellent stability, biocompatibility, and good thermal conductivity [52]. Moreover, the hydrophilic surface allows the surface modification and functionalization, which is a prerogative in any sensor application. Among the major sensing application, MXene composites have been reported as gas sensors, biosensors, wearables, etc. For example, Wang et al. [53] reported a TiO_2 modified Ti_3C_2 composite for the detection of H_2O_2. The composite showed an organ-like structure of Ti_3C_2 possessing a layered morphology resembling to that of exfoliated graphite, a suitable electrode of TiO_2–Ti_3C_2 was developed with the help of nafion binder which was beneficial for the immobilization of Hb. The specific surface area of the composite was also modified and due to these reasons, the prepared sensor showed a detection limit of 14 nM for H_2O_2. Similarly, a similar composite constituted of Ti_3C_5–Au was used for glucose detection. MXene-Au displayed the detection ability in the range of 0.1–18 mM with lower LOD at 5.9 μM. The sensing ability is attributed to the electrical conductivity of MXene, which was further enhanced by the uniform distribution of Au nanoparticle. Numerous other studies have reported the MXene-based composites for the detection of gases such as CO and CH_4. A study by Yu et al. [54] presented the adsorption of number of gases such as NH_3, H_2, CH_4, CO, CO_2, N_2, NO_2, and O_2 on the monolayer Ti_2CO_2 using the first principal simulations. It was observed that the adsorption energy of NH_3 on Ti_2CO_2 decreased significantly due to biaxial strains. When 3% biaxial strain is applied the adsorption, energy reaches to −0.51 eV indicating an effective capture on Ti_2CO_2 layer. In contrast, the adsorption energies of other gases on Ti_2CO_2 showed minor changes when biaxial strains were applied indicating weak interaction. The work discloses preferable NH_3 adsorption over other gases. The overall investigation revealed that Ti_2CO_2 could be an excellent material for detection, capture, separation, and storage of NH_3 gas. MXene composites showed high sensitivity to a varied range of physical and chemical stimuli due to their excellent physical, electrical, and optoelectronic properties. Therefore, an expected surge and significant advancements are anticipated in the research area of MXene composites as sensors.

4.3.2.3 MXene Composites for Water Pollutant Remediation

MXene composites have emerged as a promising material for the catalytic and destructive treatment of numerous conventional and recalcitrant water pollutants [55]. As discussed in previous sections, the exceptional properties of MXenes such as high specific surface area, electrical conductivity, and strong adsorption capabilities enable their possible use in conventional and non-conventional wastewater treatment techniques. They exhibit excellent adsorption capacity towards heavy metals, organic compounds, and dyes. As discussed, MXene composite showed a strong response in different photocatalytic reactions, hence, they have a tendency to be utilized in advanced oxidation processes for efficient pollutant degradation.

For example, MXene composites have been used as photocatalysts for the degradation of organic pollutants in water. The composites were able to efficiently absorb visible light and produce reactive oxygen species, which can degrade a variety of pollutants. Liu et al. [56] reported a sandwich-like Co_3O_4/MXene composite, synthesized using a hydrothermal method. The authors reported that the composite exhibited enhanced catalytic performance for the degradation of Bisphenol A in water, highlighting its potential as a heterogeneous catalyst in advanced oxidation processes. The study found that the highest catalytic activity was achieved when the Co_3O_4 loading was about 20%, outperforming both pure MXene and Co_3O_4. The catalyst also exhibited excellent stability, recoverability, and good catalytic performance across a wide pH range and in the presence of anions (NO_3^- and Cl^-). EPR and quenching tests confirmed the presence of both SO_4^{*-} and OH^* radicals in the CMs/PMS system, with SO_4^{*-} being the major oxidizing species. This discovery highlights the potential of MXene composite materials in the removal of organic pollutants and further expands the application of MXene in environmental science. Similarly, Yin et al. [57] reported novel ternary MXene composite catalyst material $Cu_2O/TiO_2/Ti_3C_2$, which exhibited efficient and sustainable catalytic activity.

Furthermore, due to their higher specific surface area, MXene composites can act as efficient adsorbents for the removal of different organic and inorganic contaminants from water or direct sewage treatment. Mashtalir et al. [58] reported a high adsorption capacity of $Ti_3C_2T_x$ for cationic methylene blue dye preferentially due to surface OH^- and hydrophilic nature. Some authors had specifically functionalized the surface of MXene to enhance its adsorption capacity, alkalization with LiOH, NaOH, and KOH was reported to take the adsorption capacity of Ti_3C_5 up to 189 mg/g. The higher capacity was attributed to intercalation of methylene blue dye into alkalized MXene.

MXene composites have shown a significant response for the treatment of different types of pollutants. Their unique properties combined with versatility in electrical and optical properties allow their usage for the efficient removal of targeted pollutants such as PFAS from water. However, continued research and development in the MXene research is important to lower the cost of production and strategies to develop new thermodynamically viable composites to enhance the removal efficiency in different water purification processes.

4.4 Conclusion

In summary, the MXene composites have been utilized as catalytic and support material in various types of reactions. These 2D materials have an excellent tendency to act as storage and electrode materials in supercapacitor and battery applications due to higher specific surface area, distinctive surface characteristics, and higher conduction-based effective ion mobility. Moreover, in light-driven reaction, the MXene composites can thrive to execute numerous uphill reactions such as water splitting and CO_2 reduction. Their role as co-catalysts is worthy of being explored in different biosensing applications. Due to the high specific surface area and excellent surface characteristics, MXene composite are suitable options to replace the conventional water treatment materials. In addition, these material composites could prove productive in destructive removal of recalcitrant pollutant from wastewater through simultaneous adsorption and advanced oxidation processes. Furthermore, for future progress, a key focus is needed on the synthesis and optimization of MXene composites to lower the cost of production and increase their catalytic efficiency.

References

1. D. Chen, W. Chen, L. Ma, G. Ji, K. Chang, J.Y. Lee, Mater. Today **17**, 184–193 (2014)
2. N. Dwivedi, C. Dhand, P. Kumar, A. Srivastava, Materials Advances **2**, 2892–2905 (2021)
3. A. Bhat, S. Anwer, K.S. Bhat, M.I.H. Mohideen, K. Liao, A. Qurashi, NPJ 2D Mater. Appl. **5**, 1–21 (2021)
4. M. Naguib, M.W. Barsoum, Y. Gogotsi, Adv. Mater. **33**, 2103393 (2021)
5. M. Naguib, M. Kurtoglu, V. Presser, J. Lu, J. Niu, M. Heon, L. Hultman, Y. Gogotsi, M.W. Barsoum, Adv. Mater. **23**, 4248–4253 (2011)
6. R.M. Ronchi, J.T. Arantes, S.F. Santos, Ceram. Int. **45**, 18167–18188 (2019)
7. A. Szuplewska, D. Kulpińska, A. Dybko, M. Chudy, A.M. Jastrzębska, A. Olszyna, Z. Brzózka, Trends Biotechnol. **38**, 264–279 (2020)
8. J. Yang, W. Bao, P. Jaumaux, S. Zhang, C. Wang, G. Wang, Adv. Mater. Interfaces **6**, 1802004 (2019)
9. A. Chroneos, D. Horlait, W. Lee, S. Middleburgh
10. Y. Luo, G.-F. Chen, L. Ding, X. Chen, L.-X. Ding, H. Wang, Joule **3**, 279–289 (2019)
11. Y. Dall'Agnese, P.-L. Taberna, Y. Gogotsi, P. Simon, J. Phys. Chem. Lett. **6**, 2305–2309 (2015)
12. S.M. George, B. Kandasubramanian, Ceram. Int. **46**, 8522–8535 (2020)
13. X. Yu, T. Wang, W. Yin, Y. Zhang, Int. J. Hydrogen Energy **44**, 2704–2710 (2019)
14. A.E. Allah, J. Wang, Y.V. Kaneti, T. Li, A.A. Farghali, M.H. Khedr, A.K. Nanjundan, B. Ding, H. Dou, X. Zhang, Nano Energy **65**, 103991 (2019)
15. Y. Liu, J. Yu, D. Guo, Z. Li, Y. Su, J. Alloy. Compd. **815**, 152403 (2020)
16. L. He, J. Liu, Y. Liu, B. Cui, B. Hu, M. Wang, K. Tian, Y. Song, S. Wu, Z. Zhang, Appl. Catal. B **248**, 366–379 (2019)
17. M.Q. Zhao, C.E. Ren, Z. Ling, M.R. Lukatskaya, C. Zhang, K.L. Van Aken, M.W. Barsoum, Y. Gogotsi, Adv. Mater. **27**, 339–345 (2015)
18. X. Liu, F. Xu, Z. Li, Z. Liu, W. Yang, Y. Zhang, H. Fan, H.Y. Yang, Coord. Chem. Rev. **464**, 214544 (2022)
19. B.C. Wyatt, B. Anasori, Appl. Mater. Today **27**, 101451 (2022)
20. H. Li, Y. Hou, F. Wang, M.R. Lohe, X. Zhuang, L. Niu, X. Feng, Adv. Energy Mater. **7**, 1601847 (2017)

21. P. Yan, R. Zhang, J. Jia, C. Wu, A. Zhou, J. Xu, X. Zhang, J. Power. Sources **284**, 38–43 (2015)
22. S. Xu, G. Wei, J. Li, W. Han, Y. Gogotsi, J. Mater. Chem. A **5**, 17442–17451 (2017)
23. T. Zhou, C. Wu, Y. Wang, A.P. Tomsia, M. Li, E. Saiz, S. Fang, R.H. Baughman, L. Jiang, Q. Cheng, Nat. Commun. **11**, 2077 (2020)
24. X. Gao, X. Du, T.S. Mathis, M. Zhang, X. Wang, J. Shui, Y. Gogotsi, M. Xu, Nat. Commun. **11**, 6160 (2020)
25. M. Carey, M. Barsoum, Mater. Today Adv. **9**, 100120 (2021)
26. J. Jimmy, B. Kandasubramanian, Eur. Polym. J. **122**, 109367 (2020)
27. D. Parajuli, N. Murali, D. KC, B. Karki, K. Samatha, A.A. Kim, M. Park, B. Pant, Polymers **14**, 3433 (2022)
28. G.J. Adekoya, O.C. Adekoya, R.E. Sadiku, Y. Hamam, S.S. Ray, ACS Omega **7**, 39498–39519 (2022)
29. X. Li, J. Hao, R. Liu, H. He, Y. Wang, G. Liang, Y. Liu, G. Yuan, Z. Guo, Energy Storage Mater. **33**, 62–70 (2020)
30. M.S. Javed, A. Mateen, I. Hussain, A. Ahmad, M. Mubashir, S. Khan, M.A. Assiri, S.M. Eldin, S.S.A. Shah, W. Han, Energy Storage Mater. (2022)
31. Y. Wang, Y. Zheng, J. Zhao, Y. Li, Energy Storage Mater. **33**, 82–87 (2020)
32. X. Wang, W. Chen, Y. Liao, Q. Xiang, Y. Li, T. Wen, Z. Zhong, J. Mater. Sci. **56**, 2486–2496 (2021)
33. W. Luo, Y. Liu, F. Li, J. Huo, D. Zhao, J. Zhu, S. Guo, Appl. Surf. Sci. **523**, 146387 (2020)
34. V.-H. Nguyen, B.-S. Nguyen, C. Hu, C.C. Nguyen, D.L.T. Nguyen, M.T. Nguyen Dinh, D.-V.N. Vo, Q.T. Trinh, M. Shokouhimehr, A. Hasani, Nanomaterials **10**, 602 (2020)
35. K. Li, T. Jiao, R. Xing, G. Zou, J. Zhou, L. Zhang, Q. Peng, Sci. China Mater. **5**, 728–736 (2018)
36. R.A. Rather, A. Mehta, Y. Lu, M. Valant, M. Fang, W. Liu, Int. J. Hydrogen Energy **46**(2021), 21866–21872 (1888)
37. R.A. Rather, M. Khan, I.M. Lo, J. Catal. **366**, 28–36 (2018)
38. M. Li, H. Huang, J. Low, C. Gao, R. Long, Y. Xiong, Small Methods **3**, 1800388 (2019)
39. X. An, W. Wang, J. Wang, H. Duan, J. Shi, X. Yu, Phys. Chem. Chem. Phys. **20**, 11405–11411 (2018)
40. J. Ran, G. Gao, F.-T. Li, T.-Y. Ma, A. Du, S.-Z. Qiao, Nat. Commun. **8**, 13907 (2017)
41. W. Yem, ChemSusChem **11**, 1606–1611 (2018)
42. Y. Zhuang, Y. Liu, X. Meng, Appl. Surf. Sci. **496**, 143647 (2019)
43. Y. Li, Z. Yin, G. Ji, Z. Liang, Y. Xue, Y. Guo, J. Tian, X. Wang, H. Cui, Appl. Catal. B **246**, 12–20 (2019)
44. Y. Li, L. Ding, Y. Guo, Z. Liang, H. Cui, J. Tian, ACS Appl. Mater. Interfaces **11**, 41440–41447 (2019)
45. X. Liu, C. Chen, Mater. Lett. **261**, 127127 (2020)
46. V. Ramalingam, P. Varadhan, H.C. Fu, H. Kim, D. Zhang, S. Chen, L. Song, D. Ma, Y. Wang, H.N. Alshareef, Adv. Mater. **31**, 1903841 (2019)
47. L. Cheng, Q. Chen, J. Li, H. Liu, Appl. Catal. B **267**, 118379 (2020)
48. M. Zhang, J. Qin, S. Rajendran, X. Zhang, R. Liu, Chemsuschem **11**, 4226–4236 (2018)
49. Y. Li, L. Ding, Z. Liang, Y. Xue, H. Cui, J. Tian, Chem. Eng. J. **383**, 123178 (2020)
50. C. Peng, P. Wei, X. Li, Y. Liu, Y. Cao, H. Wang, H. Yu, F. Peng, L. Zhang, B. Zhang, Nano Energy **53**, 97–107 (2018)
51. L. Zhang, K. Khan, J. Zou, H. Zhang, Y. Li, Adv. Mater. Interfaces **6**, 1901329 (2019)
52. D.H. Ho, Y.Y. Choi, S.B. Jo, J.M. Myoung, J.H. Cho, Adv. Mater. **33**, 2005846 (2021)
53. F. Wang, C. Yang, M. Duan, Y. Tang, J. Zhu, Biosens. Bioelectron. **74**, 1022–1028 (2015)
54. X.-F. Yu, Y.-C. Li, J.-B. Cheng, Z.-B. Liu, Q.-Z. Li, W.-Z. Li, X. Yang, B. Xiao, ACS Appl. Mater. Interfaces **7**, 13707–13713 (2015)
55. F. Dixit, K. Zimmermann, R. Dutta, N.J. Prakash, B. Barbeau, M. Mohseni, B. Kandasubramanian, J. Hazard. Mater. **423**, 127050 (2022)
56. Y. Liu, R. Luo, Y. Li, J. Qi, C. Wang, J. Li, X. Sun, L. Wang, Chem. Eng. J. **347**, 731–740 (2018)

57. J. Yin, B. Ge, T. Jiao, Z. Qin, M. Yu, L. Zhang, Q. Zhang, Q. Peng, Langmuir **37**, 1267–1278 (2021)
58. Q. Zhang, J. Teng, G. Zou, Q. Peng, Q. Du, T. Jiao, J. Xiang, Nanoscale **8**, 7085–7093 (2016)